Electronic Supplementary Material (ESI) for Materials Horizons

Optimal Vacancy Concentrations to Maximize the N–V Yield in Nanodiamonds: Electronic Supplementary Information

Amanda S. Barnard[*a]

As describe in the main text, many of the individual values for all E_d and E_Δ have been published before (and are provided in the table in the main text for convenience)and appear in references 1, 2, 3, 4 and 5.

In this case fully relaxed C_{837} and $C_{837}H_{252}$ nanodiamonds were used as initial configurations, and the various point defects were substituted for carbon atoms located along specific (albeit zigzagged) substitution paths within the lattice. The "paths" extend from the centro-symmetric atom to different points on the surfaces, edges and corners. The directions of these substitution paths are shown as dashed lines in figure 1, for substitution paths terminating at the centre of the {100} surface, {111} surface, {100}/{111} edge, {111}/{111} edge, and the {111}/{111}/{100} corner (respectively). If we consider the nanoparticle morphology as analogous to the shape of the diamond Brillouin zone, the substitution paths begin at the Γ-point and extend along the X, L, U, K and W directions, respectively. In all, the point defects were introduced at over 50 geometrically unique sites within the diamond nanoparticles, to effectively sample configuration space. Following inclusion of the defect, the entire structure was re-relaxed using the same method as described below.

All of the calculations were originally performed using density functional based tight-binding method with self-consistent charges (SCC-DFTB)[6,7] which is a two-centre approach to DFT, where the Kohn-Sham density functional is expanded to second order around a reference electron density. In this approach, the reference density is obtained from self-consistent density functional calculations of weakly confined neutral atoms, and the confinement potential is optimized to anticipate the charge density and effective potential in molecules and solids. A minimal valence basis is established and one- and two-centre tight-binding matrix elements are explicitly calculated within DFT. A universal short-range repulsive potential accounts for double counting terms in the Coulomb and exchange-correlation contributions, as well as the internuclear repulsion, and self-consistency is included at the level of Mulliken charges.[7] This method was selected in these studies as it is more computationally efficient than DFT when such as large number of individual calculations are required. In general, however, the values of the defect energies, defect energies and diffusion barriers can be generated using any simulation method, provided consistency is preserved by calculating each parameter with the same computational method and convergence criteria.

A collection of the results from previous works[1–5], using these methods, are collected in figure 2. This figure reproduces the radial distribution in the defect energies for the bucky-diamond (a) and hydrogen passivated nanodiamond (b). The relative defect energy, $E(r) - E(0)$, has consistently been used in the past, defined as the total energy of the nanoparticle with a given vacancy site relative to the energy of the nanoparticle with the vacancy in the centro-symmetric position. The x-axis represents a scaled (dimensionless) nanoparticle radius defined by dividing the distance from the centre to the average vacancy site (r_{defect}) by the total distance from the centre to the extremum (R_{total}), and averaging over each path. Hence $r_{defect}/R_{total} = 0$ is the centre, and $r_{defect}/R_{total} = 1$ is the outermost vacancy site located on a surface, edge or corner. In each case, the uncertainties in x-axis are related to the geometric differences between paths, and the uncertainties in y-axis and the statistical variance in the results, which provide a measure of instability.

Acknowledgments

Computational resources for this project were supplied by the National Computing Infrastructure (NCI) national facility under Partner Allocation Scheme, Grant q27.

References

1 A. S. Barnard, *Analyst*, 2009, **134**, 1751–1764.
2 C. Bradac, T. Gaebel, N. Naidoo, J. R. Rabeau and A. S. Barnard, *Nano Lett.*, 2009, **9**, 3555–3564.
3 A. S. Barnard and M. Sternberg, *J. Comput. Theo. Nanosci.* 2008, **5**, 2089–2095.
4 A. S. Barnard and M. Sternberg, *Nanotech.*, 2007, **18**, 025702.
5 A. S. Barnard, in *Nanodiamond*, ed. O. A. Williams, Royal Society of Chemistry, Cambridge 2014.
6 D. Porezag, Th. Frauenheim, Th. Köhler, G. Seifert and R. Kaschner, *Phys. Rev. B*, 1995, **51**, 12947.
7 Th. Frauenheim, G. Seifert, M. Elstner, T. Niehaus, C. Köhler, M. Amkreutz, M. Sternberg, Z. Hajnal, A. Di Carlo and S. Suhai, *J. Phys: Condens. Matter*, 2002, **14**, 3015.

[a] *CSIRO Materials Science and Engineering, 343 Royal Parade, Parkville, Victoria, 3052, Australia. E-mail: amanda.barnard@csiro.au*

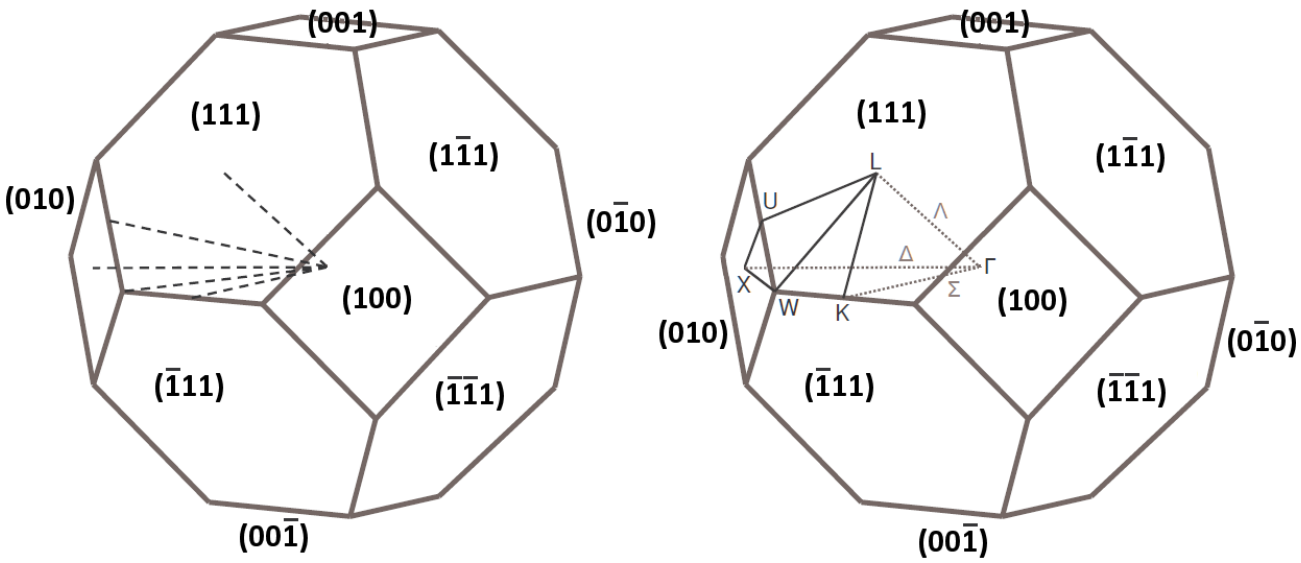

Fig. 1 Substitution paths for the inclusion of a geometrically and crystallographically diverse range of point defects in a truncated octahedral diamond nanoparticle.

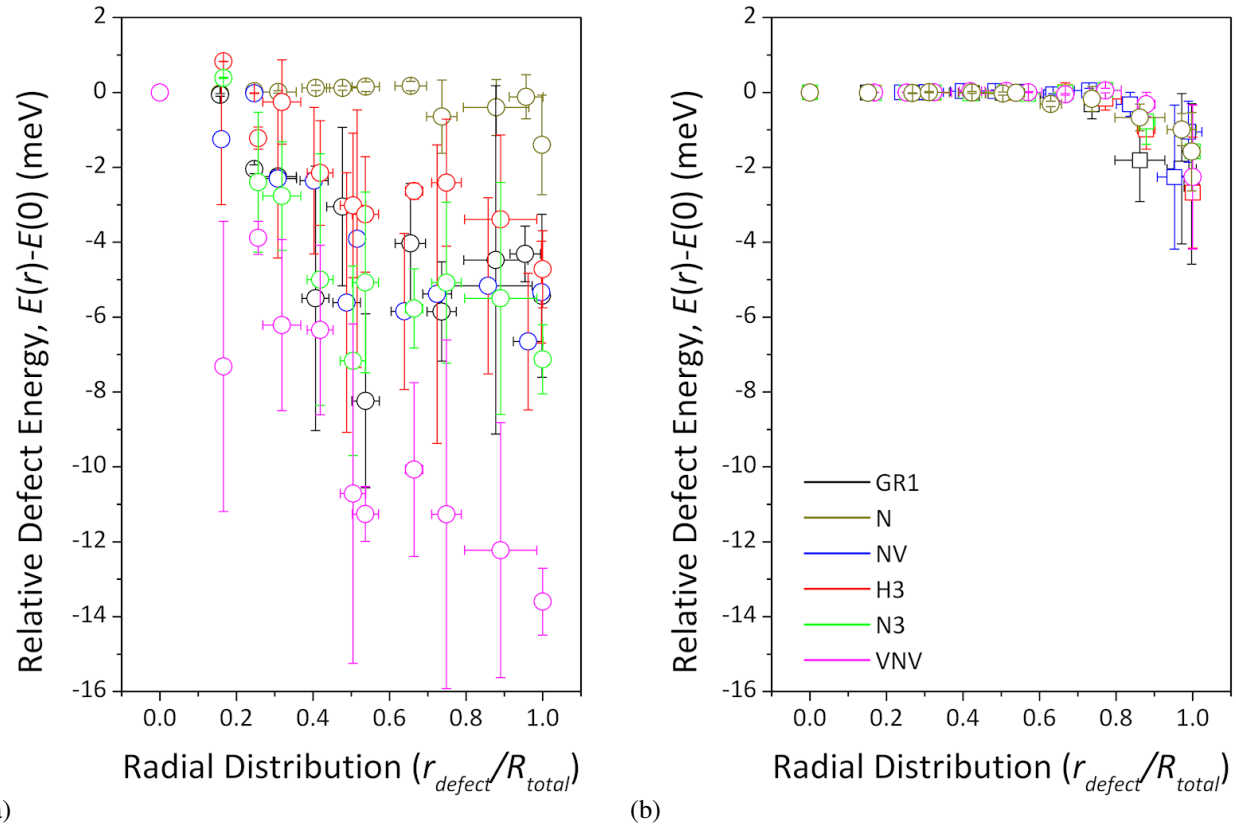

(a) (b)

Fig. 2 Stability of the GR1, N, N-V, H3, N3 and V-N-V point defects in a (a) C_{837} bucky-diamond, and (b) $C_{837}H_{252}$ nanodiamond. The legend in (b) applies to both figures.